

The intragroup medium in loose groups of galaxies

Stephen F. Helsdon^{*} and Trevor J. Ponman

School of Physics and Astronomy, University of Birmingham, Edgbaston, Birmingham B15 2TT, UK

Accepted 1999 ??; Received 1999 ??; in original form 1999 ??

ABSTRACT

We have used the *ROSAT* PSPC to study the properties of a sample of 24 X-ray bright galaxy groups, representing the largest sample examined in detail to date. Hot plasma models are fitted to the spectral data to derive temperatures, and modified King models are used to characterise the surface brightness profiles.

In agreement with previous work, we find evidence for the presence of two components in the surface brightness profiles. The extended component is generally found to be much flatter than that observed in galaxy clusters, and there is evidence that the profiles follow a trend with system mass. We derive relationships between X-ray luminosity, temperature and optical velocity dispersion. The relation between X-ray luminosity and temperature is found to be $L_X \propto T^{4.9}$, which is significantly steeper than the same relation in galaxy clusters. These results are in good agreement with preheating models, in which galaxy winds raise the internal energy of the gas, inhibiting its collapse into the shallow potential wells of poor systems.

Key words: galaxies: clusters: general – intergalactic medium – X-rays: galaxies

1 INTRODUCTION

The majority of galaxies in the universe are found in galaxy groups (Tully 1987). These collections of between 3 and about 30 galaxies trace large scale structure (Ramella, Geller & Huchra 1990) and probably contain a large fraction of the total baryonic mass in the universe (Fukugita, Hogan & Peebles 1998). However despite their abundance and importance, galaxy groups have received relatively little attention until recently. The main problem has been the identification of the groups themselves. Even when redshift information is available, it is difficult to identify whether a group is truly bound, due to the problems of small number statistics and chance superpositions. In contrast, galaxy clusters which are easier to identify due to the larger number of members, have been extensively studied.

The detection of extended X-ray emission from hot gas in the group potential well provides the best evidence that a group is truly gravitationally bound. The study of this hot intragroup gas can provide important insights into the evolution and dynamics of the group and its member galaxies. Samples of X-ray bright groups were originally studied using the *Einstein* satellite (e.g. Price et al. 1991), but the introduction of the *ROSAT* satellite with its improved sensitivity and resolution, allowed a more thorough analysis of

these systems. Since the *ROSAT* PSPC was first used to study X-ray bright groups (Mulchaey et al. 1993; Ponman & Bertram 1993) a number of collections of groups have been studied (e.g. Doe et al. 1995; Ponman et al. 1996; Burns et al. 1996; Mulchaey et al. 1996; Mahdavi et al. 1997; Mulchaey & Zabludoff 1998). However, none of these studies provides a uniform, detailed analysis of a reasonable sized sample of groups, based on high quality data. The largest samples have all been based on *ROSAT* All Sky Survey (RASS) data, in which case properties other than the luminosities are difficult to determine, due to poor statistics resulting from the short exposures.

The study of Ponman et al. (1996) used a mixture of RASS and pointed data and identified 22 X-ray bright groups. These were all compact groups from the catalogue of Hickson (1982). Such compact groups have the advantage that they can be easily identified on the sky due to the high projected over-densities of galaxies within them, but may be unrepresentative of groups as a whole. The X-ray properties of these Hickson compact groups (HCGs) showed systematic departures from those of clusters, leading to the suggestion that they might be displaying the marks of energy injection into the intergalactic medium due to galaxy winds.

Mulchaey & Zabludoff (1998) (henceforth MZ98) used pointed PSPC data to study groups of both loose and compact morphology. With a sample of only nine groups they were unable to derive reliable statistical results, however they found that properties such as the $L : T$ relation and

^{*} E-mail: sfh@star.sr.bham.ac.uk

surface brightness slope were indistinguishable from those of clusters, in contradiction to the results of Ponman et al. (1996). If this is true, it suggests a fundamental difference between the properties of loose and compact groups. The main aim of the present work is to establish the X-ray properties of loose groups by means of a careful and uniform study of a larger sample of systems, and to establish whether they do, in fact, differ from compact groups in their X-ray properties. To allow direct comparison with the results of MZ98, their sample has been included within ours.

In § 2 we describe the sample selection and initial identification of the X-ray bright groups. The spectral and spatial analyses of the X-ray emission are described in § 3 and § 4. Results of the analysis, including correlations between the derived parameters, are presented in § 5. These results are compared with those of MZ98 in § 6, and discussed in § 7. Finally, our conclusions are summarized in § 8. Throughout this paper we use $H_0 = 50 \text{ km s}^{-1} \text{ Mpc}^{-1}$.

2 SAMPLE SELECTION AND DATA REDUCTION

The primary aim of this work is to study the properties of a number of X-ray bright groups, as such it was necessary to initially compile such a sample. Three different sources were used for this purpose, the optical catalogue of Nolthenius (1993), the sample of Ledlow et al. (1996) and the X-ray bright groups from MZ98. The catalogue of Nolthenius (1993) contains 173 groups, with three or more members, selected from the CfA1 galaxy redshift catalogue using a friends of friends algorithm with a density enhancement of 15. The Ledlow et al. (1996) sample contains 71 groups selected from the Zwicky Catalogue of Galaxies and Clusters of Galaxies, using a friends of friends algorithm with a surface density enhancement of 46.4, each group having at least 4 members and galactic latitude $|b| \geq 30^\circ$.

Cross-correlation of the Nolthenius (1993) and Ledlow et al. (1996) samples with the *ROSAT* observing log, identified groups which had been observed by the *ROSAT* PSPC during its programme of pointed observations. We further restricted ourselves to groups which had been observed within $20'$ of the centre of the PSPC. The nine X-ray bright groups from MZ98 were all known to have been observed by the *ROSAT* PSPC and were added to the sample. Groups identified as being part of known bright galaxy clusters such as Coma were also excluded at this stage. This resulted in a potential sample of 37 galaxy groups, which are listed in Table 1.

Before the X-ray data can be used it is necessary to identify and exclude sources of contamination. These include particle events and solar X-ray emission scattered from the Earth's atmosphere into the telescope. Detectors on board the spacecraft identify and exclude over 99% of the particle events that would be recorded as X-rays. These particle events are recorded as the master veto rate. At values of the master veto rate of above 170 count s^{-1} the contamination by particles is significant, and these times are excluded from our analysis. Reflected solar X-rays can be identified by an increase in the total X-ray event rate. To remove this contamination, times where the total event rate deviated by

more than 2σ from the mean were excluded. Typically this resulted in the removal of a few percent of each observation.

A standard reduction of the data was then carried out to produce an image and background for each group. The statistical significance of any emission within distances of 50 kpc and 200 kpc from the optical centre of each of the groups was then calculated. This was used along with a smoothed image and a profile of the group to identify the presence of extended emission above a 5σ detection threshold. It was also apparent that in a few cases diffuse X-ray emission was centred on a galaxy within the PSPC ring, even though the catalogued optical centre of the group was outside the ring. These groups were also included, and are identified with an asterisk in Table 1. This resulted in a final sample of 24 X-ray bright galaxy groups, which are identified in Table 1. As the table shows, those systems span a considerable range in catalogued optical richness ($N_{gal} = 3 - 45$). A more reliable measure of the total mass of each group is given by the X-ray temperatures derived below. Our sample should not be regarded as being statistically complete in any way, but rather a reasonably representative sample of X-ray bright groups.

3 SPECTRAL ANALYSIS

Events surviving the initial screening process were binned into a 3-dimensional x, y, Energy data cube. An estimate of the background was generated from an annulus at $r=0.6-0.7^\circ$ with the PSPC support spokes removed. The dataset was then background subtracted, and point sources identified using a maximum likelihood source searching program. Point sources within the background annulus were removed to 1.2 times the 95% radius for 0.5 keV photons. The background was then recalculated and the image once again searched for point sources. Other more extended sources, such as background galaxy clusters not associated with the group emission, were also manually identified and excluded at this point. This process of identifying and removing point sources to produce a better estimate of the background was repeated until the same number of point sources was identified each time. Typically this took 4-5 iterations for each dataset.

The final background subtracted data were then corrected for dead time effects and vignetting, and then divided by the effective exposure time to give a map of spectral flux. A circular region around each of the groups was used to extract a spectrum. The size of this region was determined by examination of a smoothed image and a surface brightness profile of the group. The region was selected to include all the emission that could be observed in the smoothed image and profile; its size for each of the groups is shown in Table 1. Point sources, and other sources as identified above, were removed from the spectral image, along with the support structure and the data outside the radius of interest. The spectrum for each group was then obtained by collapsing the spectral image along the x and y axes.

Each spectrum was fitted with a MEKAL hot plasma model (Mewe, Lemen & van den Oord 1986) with a hydrogen absorbing column frozen at a value determined from radio surveys (Stark et al. 1992). For two of the groups it was also necessary to fix the abundance to obtain a sensible fit.

Table 1. Listed are the groups in which a search for extended X-ray emission was carried out. Groups with a 1 in the comments column have properties taken from Nolthenius (1993), those identified with a 2 are from Ledlow et al. (1996) and those marked with a 3 are from Mulchaey & Zabludoff (1998). Asterisks indicate groups in which emission was identified within the PSPC support ring, but whose catalogued optical positions were outside the ring. Groups with detected X-ray emission are listed in the top half of the table along with the radius to which emission was observed. Groups that were not used are given in the lower region of the table along with the reason for exclusion.

Name	Alt. Name	RA(2000)	Dec(2000)	N_{gal}	σ (km s $^{-1}$)	z	Comments	R_{ext} (')
NGC 315	Nol 6	00 58 25.0	+30 39 11	4	122	0.0164	1 *	6.0
NGC 383	S34-111	01 07 27.7	+32 23 59	29	466	0.0173	2	30.0
NGC 524	Nol 11	01 24 01.6	+09 27 37.7	8	205	0.0083	1	10.6
NGC 533		01 25 29.1	+01 48 17	36	464	0.0181	3	20.3
NGC 741	S49-140	01 57 00.7	+05 40 00	41	432	0.0179	3	16.0
NGC 1587	Nol 33	04 30 46.1	+00 24 25.7	4	106	0.0122	1	6.0
NGC 2563	NGC 2563	08 20 24.4	+21 05 46	29	336	0.0163	3	17.6
NGC 3091	HCG 42	10 00 13.1	-19 38 24	22	211	0.0128	3	8.9
NGC 3607	Nol 65	11 17 55.9	+18 07 35.8	3	421	0.0037	1	9.6
NGC 3665	Nol 68	11 23 30.6	+38 43 31.6	4	29	0.0069	1	6.0
NGC 4065	N79-299A,Nol 91	12 04 09.5	+20 13 18	9	495	0.0235	2	15.0
NGC 4073	N67-335	12 04 21.7	+01 50 19	22	607	0.0204	2	18.0
NGC 4261	Nol 99,N67-330	12 20 02.3	+05 20 24	33	465	0.0071	1	15.0
NGC 4325	NGC 4325	12 23 18.2	+10 37 19	18	256	0.0252	3	10.2
NGC 4636	Nol 104	12 42 57.2	+02 31 34.3	12	463	0.0044	1	21.6
NGC 4761	HGC62	12 52 57.9	-09 09 26	45	376	0.0146	3	15.6
NGC 5129	Nol 117	13 24 36.0	+13 55 40	33	294	0.0232	3	9.0
NGC 5171	N79-296	13 29 22.3	+11 47 31	8	424	0.0232	2	10.8
NGC 5353	Nol 124,N79-286,HCG68	13 51 37.0	+40 32 12	15	174	0.0081	1 *	9.6
NGC 5846	Nol 146	15 05 47.0	+01 34 25	20	368	0.0063	3	15.0
NGC 6338	N34-175	17 15 21.4	+57 22 43	7	589	0.0283	2	13.8
NGC 7176	HCG90	22 02 31.4	-32 04 58	16	193	0.0085	3	13.5
NGC 7619	Nol 164	23 20 32.1	+08 22 26.5	7	253	0.0111	1	24.0
NGC 7777	Nol 170*	23 53 33.0	+28 34 42	4	116	0.0229	1 *	6.6
NGC 7819	Nol 173	00 02 28.0	+31 28 42.1	3	71	0.0164	1 no detection	
NGC 43	Nol 1	00 13 05.8	+30 58 40.8	3	63	0.0160	1 no detection	
NGC 2769	Nol 35	09 10 22.8	+50 23 45.3	3	125	0.0166	1 no detection	
NGC 3839	Nol 82,N67-312	11 42 04.6	+10 18 20.0	9	177	0.0206	2 background clusters	
NGC 4168	Nol 98	12 13 38.9	+13 01 19.3	4	152	0.0077	1 no detection	
NGC 4360	Nol 101	12 25 44.6	+09 07 23.5	3	289	0.0245	1 behind Virgo emission	
NGC 4615	Nol 108	12 41 16.0	+26 13 33.2	3	47	0.0158	1 too few counts	
NGC 5386	Nol 129	13 58 00.1	+06 15 25.1	3	9	0.0143	1 no detection	
NGC 5775	Nol 143	14 53 24.9	+03 29 47.5	5	88	0.0051	1 no detection	
NGC 5866	Nol 147	15 16 23.5	+56 25 01.9	4	74	0.0022	1 no detection	
NGC 5970	Nol 154	15 36 16.2	+12 02 07.7	3	81	0.0064	1 no detection	
NGC 7448	Nol 160,S49-143	23 01 48.9	+15 58 09.0	8	153	0.0077	2 no detection	

A value of 0.3 solar was used for this purpose. In this way we derived temperature, abundance and bolometric flux for each group.

For hot spectra, the limited spectral band of *ROSAT* makes temperature determination subject to systematic errors in the high energy response of the PSPC, and there is evidence that *ROSAT* temperatures are systematically lower than those from hard X-ray instruments such as *Ginga* and *ASCA*. A comparison of *ROSAT* and *ASCA* temperatures by Hwang et al. 1999 showed that this temperature bias amounts to $\sim 30\%$ in hot systems, but that there is no evidence of any systematic offset below an *ASCA* derived temperature of 2keV, where the *ROSAT* band covers the spectrum adequately. We therefore expect the *ROSAT*-determined temperatures for the systems in our sample (which have $T < 1.7$ keV) to be free from serious bias.

The distribution of group temperatures in the present sample occupies a rather small range around 1 keV. For

the 22 groups in which metallicities were derived, the overall weighted mean metallicity is 0.19 ± 0.01 solar, whilst the median is 0.42 solar. A trend is observed in clusters for higher metallicity in lower temperature systems (Arnaud 1994). This would lead one to expect a typical metallicity of ≈ 0.6 solar in systems with $T \approx 1$ keV. However there is evidence that there may be abundance gradients in cool clusters which result in an increased abundance at the centre (e.g. Xu et al. 1997; Ikebe et al. 1997; Fukazawa et al. 1998; Finoguenov & Ponman 1999) and could account for the observed trend. In any case, results obtained here for the group metallicities must be viewed with caution, since *ROSAT* is unable to resolve individual emission lines, and metallicities can be strongly biased when a variable temperature plasma is fitted with an isothermal model (e.g. Buote & Fabian 1998, Finoguenov & Ponman 1999).

For each of the groups in the sample we also derived simple projected temperature profiles. In each case spectra

in several annuli were extracted and fitted with a MEKAL model as described above. In each annulus the hydrogen column and abundance were frozen at the global values. The resulting temperature profiles of all groups are shown in Fig.1. Some of the profiles shown are not particularly informative due to a combination of large errors on the temperatures and a small number of annuli. However it is clear that approximately half of the groups show evidence of a temperature drop in the central regions, indicating the presence of a cooler component. Also, approximately half of the profiles show evidence of a decline in temperature at large radii.

4 SURFACE BRIGHTNESS PROFILES AND GROUP LUMINOSITIES

Observations of galaxy clusters across a wide range in virial temperature appear to indicate a flattening of the profiles in lower mass systems (Arnaud & Evrard 1999; Ponman, Cannon & Navarro 1999) – a result consistent with expectations if the intergalactic gas has been subject to preheating by galaxy winds (Metzler & Evrard 1999; Cavaliere et al. 1999). However, MZ98 found for their sample of groups that surface brightness profiles did not differ significantly from those in clusters, once the presence of central components was properly allowed for. We set out to examine the surface brightness profiles of our group sample in an attempt to resolve this issue.

Following initial reduction, an image was extracted in the 0.5 - 2 keV band, and corrected for vignetting using an energy dependent exposure map (see Snowden et al. (1994) for description). Point sources identified in the spectral analysis were removed from the image along with any other unrelated extended sources. Only the data within the region from which each group spectrum was extracted, were used for the spatial analysis. It has been shown that the centroid of the X-ray emission often lies at the position of the brightest group galaxy (MZ98), and as such any emission centred on this galaxy may be associated with the group potential as a whole. For this reason any source associated with the centre of the X-ray emission was not removed. Use of the energy dependent exposure map to correct for vignetting, results in a constant background level across the image, therefore a flat background was also determined and subtracted from the data.

For each group the 2-dimensional surface brightness profile was modelled with a modified King function (or ‘ β -profile’) of the form:

$$S(r) = S_0(1 + (r/r_{core})^2)^{-3\beta_{fit}+0.5}$$

Models were convolved with the PSPC point spread function at an energy determined from the mean photon energy of the group spectrum, and fitted to the data. The free parameters were the central surface brightness S_0 , the core radius r_{core} , the index β_{fit} and the x and y position of the centre of the emission. Both spherical and elliptical fits were carried out on the data, with the major to minor axis ratio and the position angle being extra free parameters in the elliptical fits.

The use of 2-dimensional datasets to fit the surface brightness distribution results in a low number of counts in

many of the data bins. Under these conditions chi-squared (χ^2) fitting performs poorly, so maximum likelihood fitting, using the Cash statistic, was used instead. The Cash statistic (Cash 1979) is defined as $-2\ln L$ where L is the likelihood function (in this case derived from the Poisson distribution). Thus the most likely model has a minimum Cash statistic. Differences in the Cash statistic are χ^2 distributed, so confidence intervals may be calculated in the same way as for a conventional χ^2 fit.

Unfortunately the Cash statistic by itself gives no indication of the quality of a fit; hence it was necessary to obtain some other estimate of the fit quality. A Monte Carlo approach was used, in which the best fit model was used to simulate 1000 images of the group. Poisson noise was added to each of these images, and they were then compared to the original model, and the Cash statistic for each image determined. Thus, for a particular model we were able to obtain a distribution showing the range of Cash values expected for datasets generated from this model. A Gaussian was then fitted to this distribution to obtain the width and central value. By comparing the Cash statistic for the real dataset with this distribution, it was possible to determine the probability that the model could have produced the data. This probability is recorded in Table 2, as the number of standard deviations that the real value lies from the centre point of the distribution. If the value of the real Cash statistic lay more than 2σ from the peak of the distribution then the fit was regarded as ‘poor’.

As can be seen in Table 2, the single-component fits provide an adequate description of the data in a few cases. However for most groups the single-component fits are poor. It has been suggested that there are typically two components in the surface brightness profiles of galaxy groups (MZ98), a central component associated with a central galaxy, cooling flow or AGN, and a more extended component associated with the group potential. To check this, models comprising of two superposed β -profiles were also fitted to those datasets with poor single-component fits and greater than ≈ 900 total counts. Below this number of source counts, statistics were found to be too poor to constrain the more complicated two-component models. To limit the number of free parameters, the central component was constrained to be spherical while the outer component was allowed to vary in ellipticity.

In three of the groups (NGC4065, NGC4073 and NGC7619) the emission was bimodal, so that the two-component models fitted with the centres of the two components significantly offset from one another (e.g. see Fig.2). As a result, it is not sensible to define one component as extended, and the other as the central component. In these cases both of the components were constrained to be spherical.

The fitted parameters of the two-component King profiles are also shown in Table 2, along with an estimate of the goodness of fit. The errors quoted are 1σ for one interesting parameter. Note that these errors are only reliable for reasonable fits (see final column in Table 2). The best fitting surface brightness profiles were also used to correct the derived group fluxes for the diffuse emission lost when point sources are removed. A model image for the group was produced, and from the ratio of the number of counts in the model image to that in the same image with ‘holes’ punched

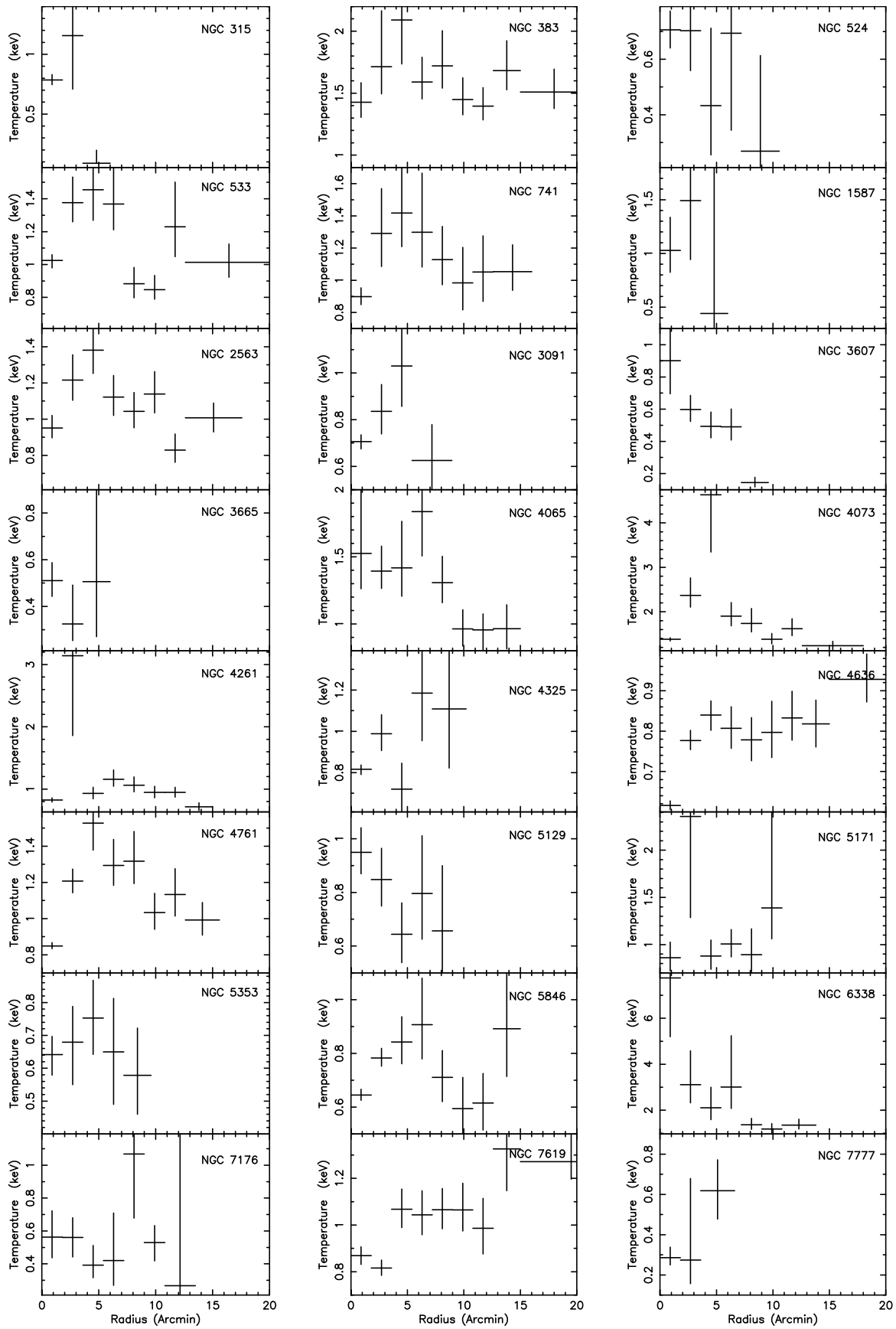


Figure 1. Temperature profiles from an annular analysis of the 24 groups in this sample. A number of the groups show a temperature drop in the central regions and/or at large radii.

Table 2. Results of the surface brightness fits for elliptical and two-component models. If two models are shown for a group, the first is the elliptical model and the second the the two-component model. Models marked with an * are groups in which two separate centres of emission could be observed. The goodness of fit is as described in the main body of the text. All errors are 1σ for one interesting parameter.

Group	Extended component				Central component		Goodness of fit
	β_{fit}	Core radius (arcmin)	Axis ratio	Position angle (degrees)	Core radius	β_{fit}	
NGC 315	1.37 ± 0.36	0.42 ± 0.10	1.08 ± 0.13	141 ± 65	-	-	-0.5
NGC 383	0.362 ± 0.003	0.43 ± 0.06	1.34 ± 0.05	166 ± 4	-	-	8.2
	0.48 ± 0.02	6.9 ± 0.9	1.19 ± 0.04	156 ± 6	0.01 ± 0.03	0.48 ± 0.02	5.2
NGC 524	0.45 ± 0.01	0.01 ± 0.01	1.41 ± 0.22	143 ± 16	-	-	18.2
NGC 533	0.482 ± 0.005	0.40 ± 0.03	1.60 ± 0.06	77 ± 3	-	-	14.2
	0.75 ± 0.14	10.2 ± 2.8	1.89 ± 0.04	49 ± 2	0.02 ± 0.02	0.54 ± 0.02	-0.23
NGC 741	0.465 ± 0.008	0.37 ± 0.05	1.35 ± 0.09	74 ± 6	-	-	11.2
	0.391 ± 0.009	0.10 ± 0.13	1.24 ± 0.11	174 ± 11	0.17 ± 0.09	0.9 ± 0.3	0.20
NGC 1587	0.47 ± 0.06	0.34 ± 0.27	1.4 ± 0.5	35 ± 22	-	-	-0.1
NGC 2563	0.369 ± 0.003	0.01 ± 0.02	1.28 ± 0.04	88 ± 7	-	-	4.6
	0.400 ± 0.004	2.6 ± 0.6	1.31 ± 0.06	95 ± 7	0.2 Fixed	1.0 Fixed	1.54
NGC 3091	0.60 ± 0.02	0.48 ± 0.06	1.64 ± 0.09	14 ± 4	-	-	10.0
	0.41 ± 0.02	0.1 ± 0.05	4.3 ± 1.3	184 ± 4	0.3 ± 0.07	0.66 ± 0.05	0.82
NGC 3607	0.52 ± 0.18	4.8 ± 1.2	3.4 ± 0.7	20 ± 3	-	-	3.2
*	0.45 ± 0.04	0.28 ± 0.16	1.0 Fixed	0.0 Fixed	0.01 ± 0.04	0.38 ± 0.03	0.63
NGC 3665	0.49 ± 0.03	0.13 ± 0.12	1.4 ± 0.2	63 ± 19	-	-	0.2
NGC 4065	0.47 ± 0.04	4.1 ± 0.6	3.6 ± 0.4	7 ± 1	-	-	8.9
*	0.41 ± 0.01	0.05 ± 0.06	1.0 Fixed	0.0 Fixed	4.3 ± 1.4	0.8 ± 0.2	2.49
NGC 4073	0.431 ± 0.002	0.10 ± 0.01	1.25 ± 0.02	103 ± 3	-	-	2.5
	0.46 ± 0.01	2.14 ± 0.26	1.28 ± 0.04	102 ± 4	0.34 ± 0.05	0.73 ± 0.06	1.64
NGC 4261	0.446 ± 0.004	0.01 ± 0.01	1.34 ± 0.09	47 ± 5	-	-	13.6
	0.35 ± 0.03	3.3 ± 1.0	1.22 ± 0.13	156 ± 17	0.28 ± 0.01	1.0 Fixed	-1.20
NGC 4325	0.60 ± 0.01	0.32 ± 0.03	1.17 ± 0.05	11 ± 8	-	-	1.3
NGC 4636	0.476 ± 0.003	0.268 ± 0.014	1.09 ± 0.08	17 ± 7	-	-	17.0
	0.373 ± 0.008	0.013 ± 0.006	1.15 ± 0.06	167 ± 9	0.92 ± 0.11	0.81 ± 0.06	6.39
NGC 4761	0.502 ± 0.005	0.30 ± 0.02	1.33 ± 0.04	16 ± 3	-	-	19.3
	0.364 ± 0.006	0.10 ± 0.04	1.17 ± 0.09	72 ± 14	0.49 ± 0.06	0.85 ± 0.04	1.28
NGC 5129	0.44 ± 0.01	0.15 ± 0.06	1.30 ± 0.16	28 ± 13	-	-	-0.7
NGC 5171	0.34 ± 0.03	0.84 ± 0.71	2.7 ± 0.9	171 ± 6	-	-	0.8
NGC 5353	0.58 ± 0.03	1.35 ± 0.17	1.34 ± 0.11	129 ± 7	-	-	71.0
	0.44 ± 0.02	0.29 ± 0.13	1.8 ± 0.2	25 ± 5	0.01 ± 0.01	1.0 Fixed	6.39
NGC 5846	0.66 ± 0.02	1.43 ± 0.08	1.70 ± 0.05	246 ± 2	-	-	106.9
	0.58 ± 0.01	0.84 ± 0.07	1.16 ± 0.03	47 ± 7	0.27 ± 0.04	1.0 Fixed	3.48
NGC 6338	0.423 ± 0.004	0.06 ± 0.01	1.24 ± 0.06	24 ± 7	-	-	21.9
	0.52 ± 0.04	2.6 ± 0.4	1.29 ± 0.07	23 ± 6	0.42 ± 0.03	1.0 Fixed	1.40
NGC 7176	1.07 ± 0.29	8.0 ± 4.2	1.6 ± 0.2	139 ± 10	-	-	2.3
NGC 7619	0.458 ± 0.006	1.42 ± 0.08	1.93 ± 0.07	210 ± 1	-	-	22.7
*	0.78 ± 0.08	0.26 ± 0.05	1.0 Fixed	0.0 Fixed	0.01 ± 0.01	0.40 ± 0.01	6.27
NGC 7777	0.35 ± 0.02	0.01 ± 0.01	1.0 Fixed	0.0 Fixed	-	-	1.1

at the positions of detected sources, a correction factor for the fluxes was obtained. The luminosity of each group was then calculated using distances corrected for infall to Virgo and the Great Attractor (Fixsen et al. 1996; Burstein 1990), which are listed in Table 3.

In the case of groups with a detected central component, we checked for the possibility that this might arise from a nuclear source in the central galaxy. Fits with Gaussian models for the central component show that it is extended at $> 99\%$ confidence in all cases except NGC 5353, where statistics are too poor to constrain the extent of the central source. For each of these systems a search for radio sources associated with the brightest group galaxies was carried out using NED and the Burns et al. 1987 radio survey of groups, which has some overlap with this sample. This search identified radio sources associated with six of the brightest group galaxies: NGC 383, NGC 741, NGC 4261, NGC 4636, NGC 5353 and

NGC 6338. Hwang et al. 1999 have studied three of these using ASCA spectra. Two showed no significant improvement in fit statistic when a powerlaw component was added to the spectral model. For the third, NGC 6338, Hwang et al. 1999 find evidence that there may be contamination by an AGN, although in our data the spatial extent of the central component in this, and almost all the other systems rules out a large AGN component. The only system that may be contaminated (as indicated by the spatial extent of the central component) is NGC 5353. For this system we fitted the spectral data for this group with an added power-law component of index 1.7. We then calculated the relative contributions from the power-law and hot plasma components in the *ROSAT* band. This showed that even for the 90% upper limit of the power-law component the emission was dominated by the hot plasma component. Our conclusion from these spatial and spectral studies is that any AGN contri-

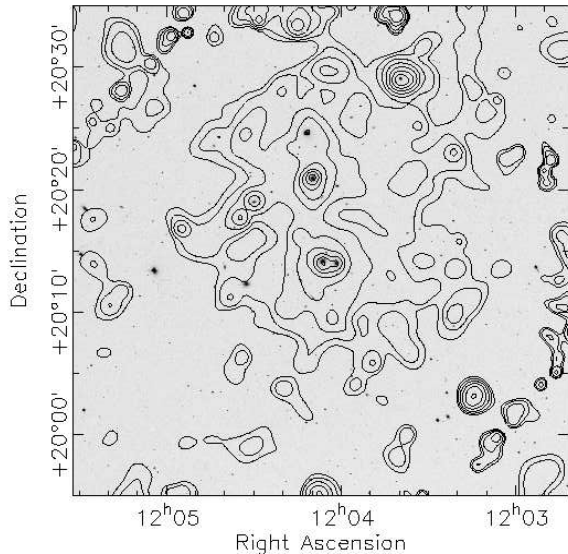


Figure 2. Contours of adaptively smoothed X-ray emission from the group NGC4065, overlaid on an optical image. It is clear that there are two distinct centres of emission in this system.

tribution to the central components in these systems appears to be minor.

We were also interested in the way in which the luminosity of groups varies with radius. The model images were therefore used to calculate luminosities within radii of 200 kpc, 500 kpc, 1/3 of the virial radius and the virial radius (R_V). Note that R_V lies well beyond the radius to which significant X-ray emission can actually be detected in our data, in almost all cases. It can be seen in Table 2 that the two-component models provide good descriptions of the data in the majority of cases. However even in the cases where the two-component fit is not acceptable it is significantly better than the single-component model, thus where possible, the two-component models are used for the purposes of calculating the effects of extrapolating to different radii. The virial radii of the groups were determined using the relation obtained from simulations by Navarro, Frenk & White (1995). This is given (for $H_0 = 50 \text{ km s}^{-1} \text{ Mpc}^{-1}$) by,

$$R_V = 2.57 \left(\frac{T}{5.1 \text{ keV}} \right)^{\frac{1}{2}} \text{ Mpc}.$$

Luminosities and temperatures derived in this study are generally similar to those from earlier studies (Doe et al. 1995; Ponman et al. 1996; Mulchaey et al. 1996; Burns et al. 1996; Mulchaey & Zabludoff 1998). The small differences in the luminosities of groups common to both this sample and that of Burns et al. (1996) are most likely primarily due to the fact that Burns et al. (1996) use a spectral model with a temperature of 1 keV to derive all luminosities, whereas the luminosities derived here use fitted spectral models, and thus should be more reliable.

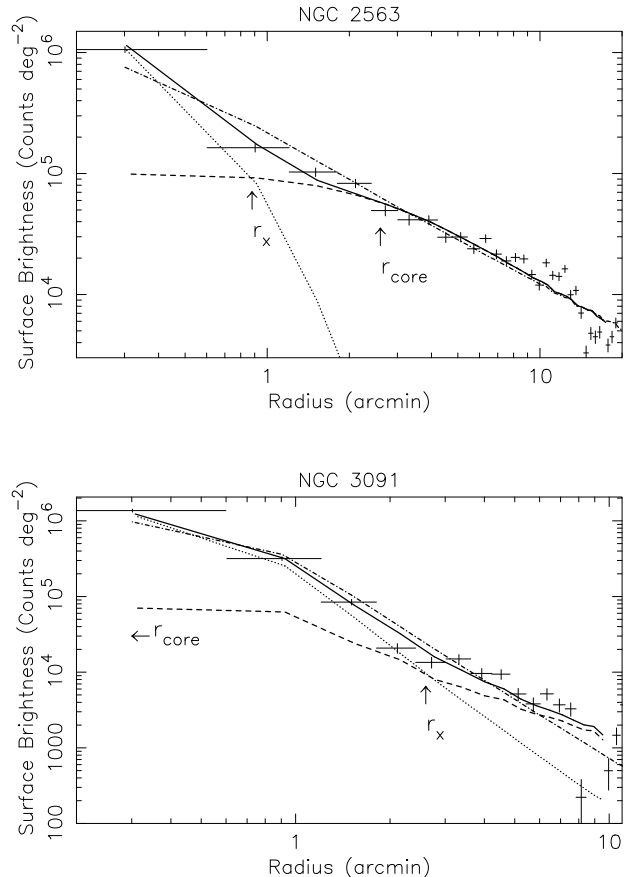


Figure 3. 1D surface brightness profiles for the groups NGC 2563 and NGC 3091. The overall best fit two component models are shown as the solid lines, with the dotted line representing the central component and the dashed line the extended. Data points are shown as crosses. For comparison the single component elliptical models are marked as the dot-dashed lines. This is steeper than the extended component in NGC 3091 but slightly flatter than it in NGC 2563. r_{core} marks the core radius of the extended component and r_x the crossover radius, as defined in the text.

5 RESULTS

Throughout the following sections, the luminosities quoted are extracted from within the radius given in Table 3. Corrections for removed point sources have been made using the best model derived for each group; either two-component or (elliptical) single-component.

5.1 X-ray profiles

The surface brightness profiles for our 24 systems break down into 12 two-component, 9 single-component and 3 bimodal cases. However, note that the nine single-component systems include the eight groups with the lowest source counts in the sample, so it is likely that the majority of these single-component fits appear to be adequate only because of poor statistics. Two examples of radial profiles are shown in Fig.3. These 1D profiles only give an approximate representation of our 2D models, but the centres of the two components almost coincide in the two cases shown, and

Table 3. Results of the spectral fitting are shown along with the derived luminosities for each of the groups. The distance to each of the groups is calculated after allowances for infall to Virgo and the Great Attractor. The luminosities are those derived within the radius to which emission could be observed. The final column shows what fraction of the luminosity as extrapolated to the virial luminosity is observed within the stated radius. All errors are 1σ .

Group name	N_H (1.0^{21} cm^{-2})	Temperature (keV)	Abundance (Solar)	Distance (Mpc)	log L (erg s^{-1})	Radius of extraction (arcmin)	Physical radius (kpc)	Fraction of virial luminosity
NGC 315	0.588	0.85 ± 0.07	0.12 ± 0.05	96.4	42.15 ± 0.15	6.0	168	1.00*
NGC 383	0.54	1.53 ± 0.07	0.40 ± 0.09	101.8	43.31 ± 0.02	30.0	889	0.76
NGC 524	0.467	0.56 ± 0.08	0.35 ± 0.43	49.9	41.37 ± 0.11	10.6	153	0.59
NGC 533	0.305	1.06 ± 0.04	0.82 ± 0.19	106.8	42.95 ± 0.02	20.3	630	0.91
NGC 741	0.442	1.08 ± 0.06	0.48 ± 0.18	106.0	42.66 ± 0.03	16.0	494	0.59
NGC 1587	0.692	0.92 ± 0.15	0.3 Fixed	77.1	41.50 ± 0.18	6.0	134	0.46
NGC 2563	0.424	1.06 ± 0.04	0.56 ± 0.14	106.7	42.79 ± 0.02	17.6	546	0.57
NGC 3091	0.478	0.71 ± 0.03	0.95 ± 1.08	90.6	42.20 ± 0.03	8.9	236	0.81
NGC 3607	0.156	0.41 ± 0.04	0.05 ± 0.02	33.1	41.59 ± 0.03	9.6	92	0.34
NGC 3665	0.204	0.45 ± 0.11	0.17 ± 0.14	52.5	41.36 ± 0.10	6.0	92	0.66
NGC 4065	0.239	1.22 ± 0.08	0.80 ± 0.36	151.3	42.99 ± 0.04	15.0	660	0.76
NGC 4073	0.190	1.59 ± 0.06	0.94 ± 0.12	135.9	43.70 ± 0.01	18.0	711	0.75
NGC 4261	0.156	0.94 ± 0.03	0.20 ± 0.02	53.0	42.32 ± 0.02	15.0	231	0.26
NGC 4325	0.223	0.86 ± 0.03	2.01 ± 1.09	162.6	43.35 ± 0.03	10.2	482	0.95
NGC 4636	0.179	0.72 ± 0.01	0.51 ± 0.04	32.8	42.48 ± 0.01	21.6	206	0.46
NGC 4761	0.297	1.04 ± 0.02	0.36 ± 0.04	104.7	43.16 ± 0.01	15.6	475	0.59
NGC 5129	0.176	0.81 ± 0.06	0.51 ± 0.22	149.9	42.78 ± 0.04	9.0	393	0.65
NGC 5171	0.193	1.05 ± 0.11	0.40 ± 0.20	150.1	42.92 ± 0.05	10.8	472	0.39
NGC 5353	0.0973	0.68 ± 0.05	0.30 ± 0.07	58.0	41.76 ± 0.03	9.6	162	0.46
NGC 5846	0.428	0.70 ± 0.02	0.43 ± 0.10	42.3	42.36 ± 0.02	15.0	185	0.88
NGC 6338	0.256	1.69 ± 0.16	0.06 ± 0.04	171.2	43.93 ± 0.01	13.8	687	0.79
NGC 7176	0.163	0.53 ± 0.11	0.3 ± 0.6	50.6	41.47 ± 0.11	13.5	199	0.90
NGC 7619	0.496	1.00 ± 0.03	0.44 ± 0.09	64.9	42.62 ± 0.02	24.0	453	0.59
NGC 7777	0.500	0.62 ± 0.15	0.3 Fixed	133.4	41.75 ± 0.20	6.6	256	0.32

* NGC 315 fits with a high β_{fit} and it is possible that for this group the emission may be due to a extensive elliptical galaxy halo rather than genuine group emission.

profiles for both data and model components have been derived about the centre of the more compact component. A distinct ‘shoulder’ in the observed profile indicates the need for two components in the model, as noted by MZ98.

The median value of β_{fit} obtained for the extended group component in our sample (from two-component fits where available, or else single-component fits), is $\beta_{fit} = 0.46$, and the weighted mean is 0.42 ± 0.06 (where the error is derived from the scatter of the values about the mean). This value of β_{fit} can be compared with the typical value for rich clusters, $\beta_{fit} \approx 2/3$ (Arnaud & Evrard 1999; Mohr, Mathiesen & Evrard 1999), indicating that the surface brightness profiles of the groups in this sample are generally significantly flatter than those of clusters.

In the case of a number of the groups, the core radius derived for the extended group component is smaller than the resolution of the *ROSAT* PSPC. Such a small core radius means essentially that the group emission has been fitted with a power law model. In such cases, the derived core radii are unreliable, particularly if an additional central component is present. To investigate the effect of a small core radius on the other derived parameters, in particular the slope, β_{fit} , we varied the core radii in a number of groups which fitted with two components and a small core radius for the extended component. It was found that varying the core radii between 0.1 and 1.0 arcmin typically changes the value of β_{fit} by less than 5%. Values of the index and core radius of the central component also varied only within 1σ

of their best fit values. Hence uncertainties in core radius in such cases do not seriously compromise our results for other parameters.

We define the ‘cross-over radius’, r_x , to be the radius within which the central component dominates the surface brightness. We derived values for r_x for the twelve groups for which two-component fits were available, but the emission was not bimodal. The mean cross-over radius for these systems was $r_x = 35 \pm 6$ kpc. Groups with two-component profiles which have $r_{core} < r_x$ are deemed to have poorly determined core radii. In order to gain some insight into the typical core radii of galaxy groups, the median value was determined, using r_x as an upper limit for those groups with $r_{core} < r_x$. Under these assumptions the median core radius of the twelve groups was found to be 60 kpc.

The relationship between the integrated temperature of the intragroup gas and the best obtained β_{fit} value for each of the groups is plotted in Fig.4. Also shown are cluster data from Arnaud & Evrard (1999) (data points with circles). The group data are split into two categories: single-component (plain crosses) and the extended component from the two-component fits (points with square in centre). As can be seen, the general trend in clusters is for β_{fit} to drop with decreasing temperature. In the region of the graph containing the group data it is clear that the majority of the groups have low β_{fit} values, but there is also a large amount of scatter, in particular amongst the groups with single-component fits.

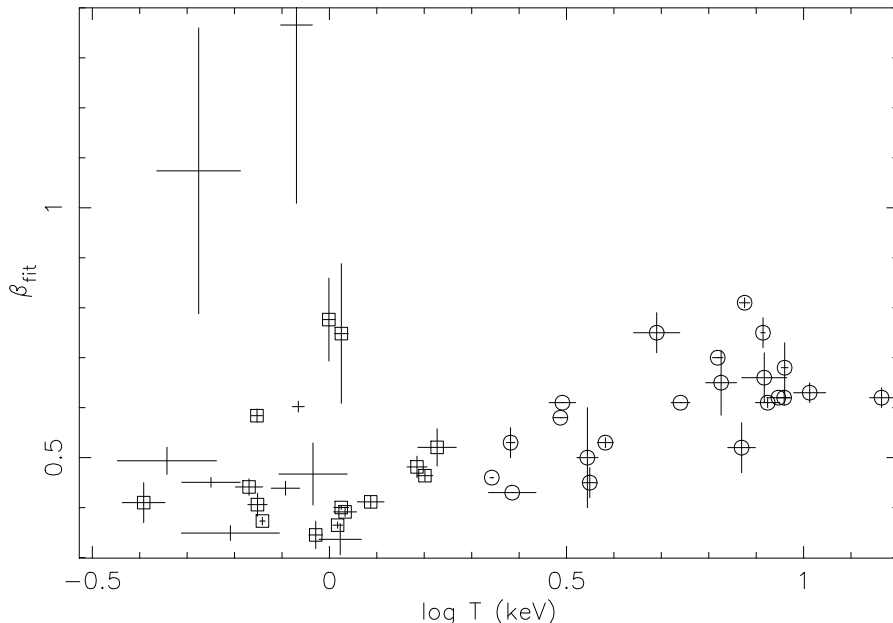


Figure 4. The relationship between β_{fit} and temperature for the whole group sample compared to cluster data from Arnaud & Evrard (1999). Values from groups with single-component fits are shown as plain crosses, those from two-component fits as crosses with central squares. The cluster data are marked as crosses with central circles.

Fig.4 also includes the three bimodal groups. Excluding these three groups, the single-component fits and the two-component fits whose quality of fit (from the Monte Carlo simulations) is poor, greatly reduces the scatter in the group results. The outcome is a much clearer trend in β_{fit} with temperature, as can be seen in Fig.5. The combined groups and cluster data are significantly correlated with a Kendall's rank correlation coefficient (a distribution free test for correlation) of $K=4.05$ ($P=0.00006$ of chance occurrence). The one group point that conflicts with the general trend (NGC533) is, in fact, the only group in the sample which has a flatter β_{fit} value for its central component than for the extended component. This means that the central component has a significant effect beyond the central region. Hence the *shape* of this component could affect the parameters obtained for the extended component. To test this, we refitted the surface brightness profile with a Gaussian model for the central component, in place of the previous King model. The β_{fit} value for the extended component changed markedly, and the new value is denoted by the triangle in Fig.5. As can be seen, this point is now much closer to the trend described by the other groups.

5.2 Luminosity, temperature and velocity dispersion

5.2.1 X-ray luminosities

Bolometric luminosities for each group, derived from within the extraction radius as described in section 3, are given in Table 3, along with best fit spectral properties. The tabulated luminosities are those of the intragroup gas only. Errors on the luminosities are derived from Poisson errors on

the data combined with errors arising from uncertainties in the fitted surface brightness profiles, which are used to correct for flux lost where contaminating sources have been excluded.

The flat surface brightness profiles of groups imply that a significant fraction of their luminosity derives from large radii. To quantify this, we used our best fit surface brightness models to derive bolometric luminosities extrapolated to R_V , and the fraction of this luminosity represented by the luminosity derived from within the extraction radius is shown for each group in Table 3. This may be as low as $\sim 30\%$ in some cases.

The effect of scaling the luminosities to different radii is shown in more detail in Fig.6. This analysis is based on the eight systems with well-fitting two-component profiles. These have been binned into three temperature bins to reduce fluctuations from system to system and show trends more clearly. The luminosity as a fraction of that within R_V is shown at three radii for the systems within each temperature bin. Points marked by triangles (dash-dot-dot line) show these ratios at a radius of 200 kpc, squares (dashed line) at the radius out to which emission could be detected, and crossed circles (solid line) at one third of the virial radius of the group. As can be seen the luminosity is significantly underestimated in all cases. In particular, for groups measured to a fixed radius of 200 kpc, and for the coolest groups at the extraction radius, one may underestimate L_X by factor of more than two.

5.2.2 Correlations

The well-known relation between X-ray luminosity and temperature is apparent in our sample. The two parameters are

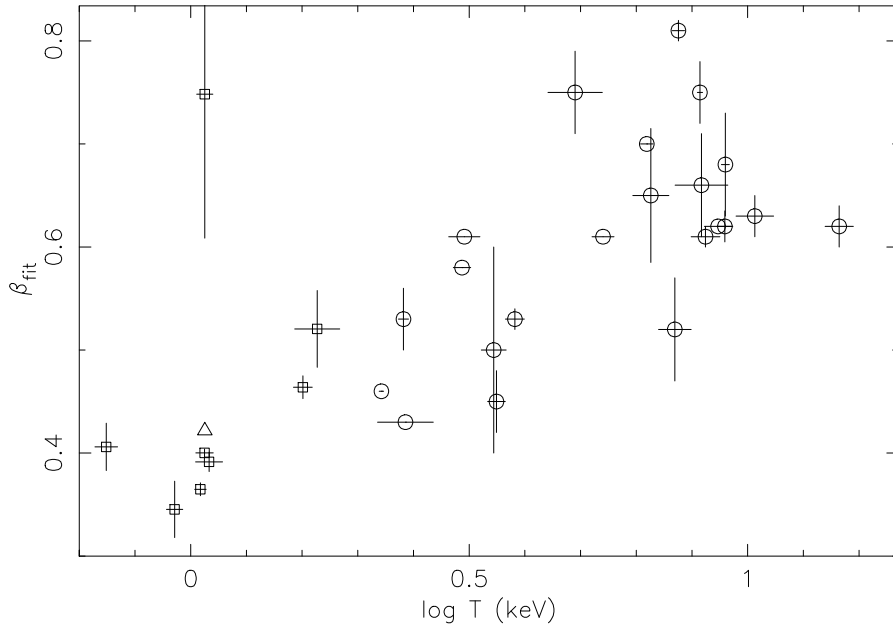


Figure 5. The relation between β_{fit} and temperature for a subsample of the groups with the best two-component models, and the cluster data. Symbols are the same as in the previous figure. The triangle marks the new value of the one discrepant group value when its central component was refitted with a Gaussian.

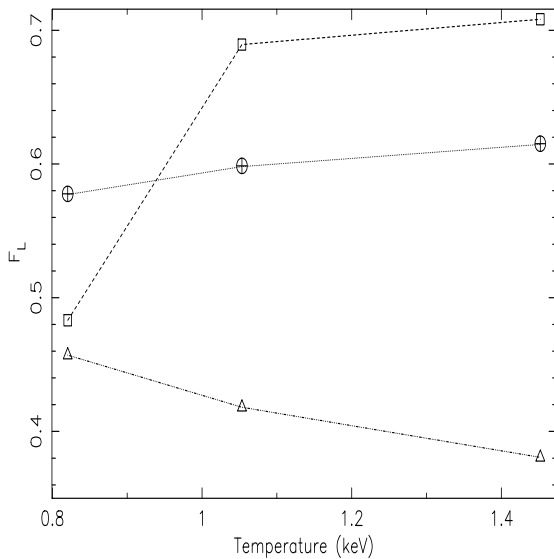


Figure 6. Fraction of the total luminosity observed within three different radii, as deduced from best fitting surface brightness models, for systems of different temperature. Squares show the luminosity within the radius to which emission could be observed, circles the luminosity within $R_V/3$, and triangles the luminosity within a fixed radius of 200 kpc.

significantly correlated ($K=4.81$, $P<0.00001$) and the relation between them is shown in Fig.7. Neither the errors on L_X or T are negligible, and a doubly weighted technique made available through the ODRPACK package was used in

this and following plots to determine the best fit line,

$$\log L_X = (42.98 \pm 0.08) + (4.9 \pm 0.8) \log T .$$

This relationship is marked with its 1σ error bounds in Fig.7. A best fit to the cluster $L : T$ relation has been derived by White, Jones & Forman (1997). They obtain $\log L_X = 42.67 + 2.98 \log T$, which is marked as the heavy dashed line in Fig.7. This line is much flatter than the best trend fit for the loose groups.

The luminosities used in this plot are those within the radius of extraction. Fig.6 shows that at this radius the luminosities will be underestimated, with the effect being greatest in the smaller mass systems. This means that if luminosities extrapolated to the virial radius were used, the $L : T$ slope should be slightly flatter. This is indeed found to be the case, with a best fitting relation of $\log L_X = (43.17 \pm 0.07) + (4.2 \pm 0.7) \log T$, although the difference in slope from the previous relation is not formally significant.

If galaxy systems scaled with mass in a self-similar way, then one would expect $L_X \propto T^2$. The cluster relation is steeper than this, and our result for groups is steeper still. However, the relationships derived by White et al. (1997) do not take into account the effects of cluster cooling flows, and recent work suggests that the $L : T$ relation may be flattened towards $L_X \propto T^2$ when the effects of cooling flows are allowed for (Allen & Fabian 1998; Markevitch 1998). Such a flattening of the relation for clusters would raise its extrapolation at low temperatures, accentuating the disagreement with the low luminosities observed in groups.

In Fig.8, velocity dispersion is plotted against the X-ray luminosity for our sample. A strong correlation can be seen

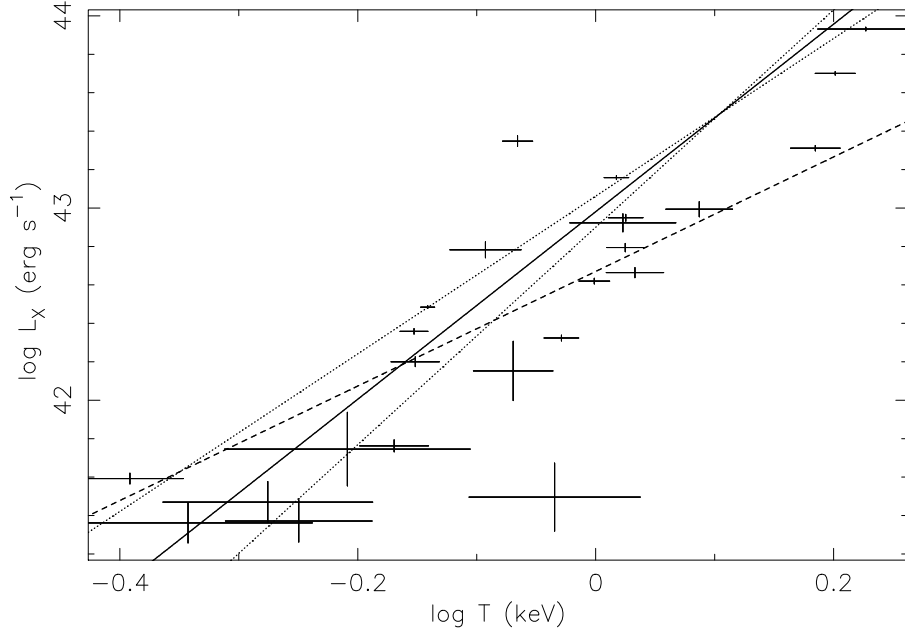


Figure 7. The relation between X-ray luminosity and temperature for our group sample. The solid line shows the best fit relation to our data, with one sigma error bounds marked by dotted lines. The extrapolation of the best fitting cluster relation (White et al. 1997) is shown as the dashed line.

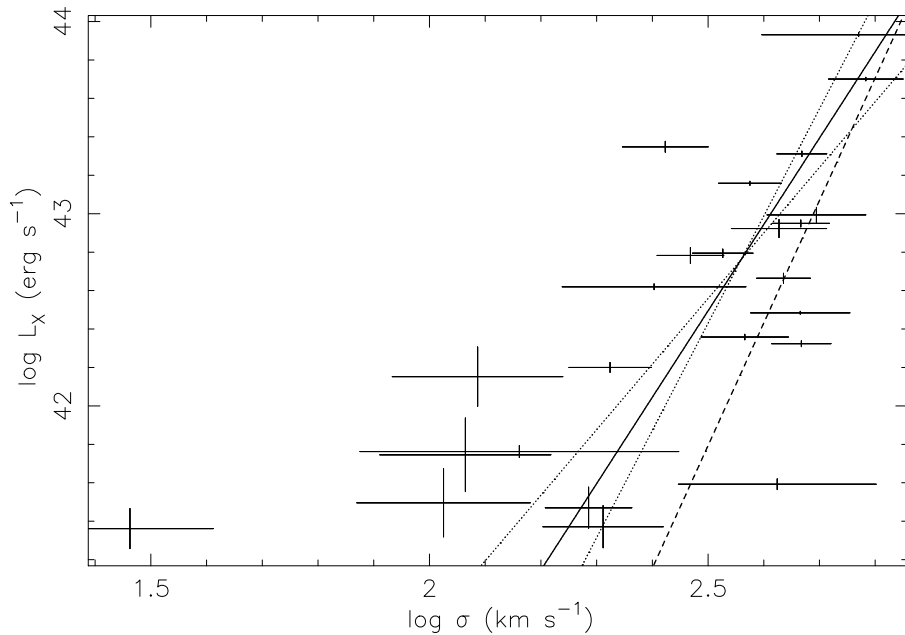


Figure 8. The relationship between X-ray luminosity and group velocity dispersion, σ . The best fit to the data is shown as the solid line with the one sigma error bounds marked by the dotted lines. The extrapolation of the cluster relation (White et al. 1997) is shown as the dashed line.

between these two parameters ($K=3.97$, $P=0.00006$). A regression line fitted to the data gives

$$\log L_X = (31.3 \pm 2.8) + (4.5 \pm 1.1) \log \sigma ,$$

which is marked in Fig.8 with its 1σ error bounds. This relationship is somewhat flatter than the cluster trend given by White et al. (1997) of $\log L_X = 25.84 + 6.38 \log \sigma$ (bold dashed line in Fig.8). Dell'Antonio, Geller & Fabricant (1994) found evidence that the $L : \sigma$ relation may flatten

below $\sigma \approx 300 \text{ km s}^{-1}$. However they did not remove the galaxy contribution from the X-ray emission, and suggest that their flattening may arise from the galaxy contribution becoming significant at low luminosities. This flattening has also been confirmed by Mahdavi et al. (1997). In the work presented here, contaminating sources were removed, but a flatter relation than clusters is still seen. Our result is actually consistent with that expected from self similar scaling of clusters, i.e. $L_X \propto \sigma^4$. However, errors are large and there is a good deal of scatter, so that the disagreement with the cluster result is not highly significant, and requires further confirmation.

A strong correlation between σ and T is shown in Fig.9 (K=3.82, P=0.0001). A regression line fitted to the data gives

$$\log \sigma = (2.57 \pm 0.03) + (1.1 \pm 0.2) \log T ,$$

which is shown in Fig.9 with its 1σ error bounds. Also shown in Fig.9 is the line $\beta_{spec} = 1$, where β_{spec} is defined as the ratio of the specific energy in the galaxies to that in the gas. As can be seen, this $\beta_{spec} = 1$ line is flatter than the relation for the loose group sample. However it is interesting to note that the higher temperature groups appear to be consistent with $\beta_{spec} = 1$, while the lower temperature groups appear to fall well below this relation. The extension of the best fit relation for galaxy clusters as determined by White et al. (1997) is shown as the dashed line in Fig.9. This line, given by $\log \sigma = 2.53 + 0.6 \log T$, is also significantly flatter than the relation determined for the loose group sample.

The unweighted mean value of β_{spec} for our sample is 0.86 ± 0.13 . However, with one exception, it is clear that β_{spec} is decreasing in the lower temperature (i.e. lower mass) systems. These results are in good agreement with those of Bird, Mushotzky & Metzler (1995), who predict a trend towards lower β_{spec} in smaller systems.

The one low temperature point (NGC 3607) that has a high velocity dispersion is also deviant in the $L : \sigma$ plot. Examination of the group members reveals that, of the three catalogued members, one is a large angular distance from the remaining two, and has a large difference in recession velocity. Also there is a further bright galaxy at the redshift of the group, which is very close to two of the catalogued members. The recession velocity of this galaxy is between those of the two catalogued galaxies, and is almost certainly a group member, although it was not classified as such by Nolthenius (1993). These two effects combined indicate that the true velocity dispersion of the group is probably considerably lower than our estimate, which is taken from Nolthenius (1993).

6 COMPARISON WITH MULCHAEY AND ZABLUDOFF

As discussed in the introduction, we have included the X-ray bright systems studied by MZ98, in order to allow a direct comparison of our results with theirs. This is important, since our conclusions about β_{fit} , β_{spec} and the $L : T$ relation all differ from MZ98. In Table 4 we show the best fit parameters as determined by MZ98 for the groups that both they and we fit with two-component models (Note

that they also fit two component models to NGC 4325 and NGC 5129, whilst we find that single component elliptical models provide an adequate representation of our data for these systems). Whilst we confirm their conclusion that two-component fits are required to adequately represent most systems, it can be seen there are some significant differences between the two sets of results.

The fitting techniques used by MZ98 differ from those used in this work. Since they work with radial profiles, their fits are necessarily 1D models, with both components centred at the same point. Their method firstly involved excluding the central region and fitting for the outer component only. The central component was then fitted with the extended component fixed at the values derived from the previous fit. Thus at no stage were the two components allowed to fit simultaneously. The 2D models fitted in this work allow the positions of the two components to vary and also permit elliptical models to be used. Parameters for the two components were also optimised simultaneously. The lower number of counts in each bin forced us to use maximum likelihood fitting rather than χ^2 fitting, but the quality of the fits were checked using the Monte Carlo approach as described above.

To demonstrate the dangers of a 1D approach to fitting the surface brightness profiles we simulated an image of a group, in which the outer component was elliptical (axis ratio=1.5), and offset a short distance (3 arcmin) from the central component. These values were chosen to construct a fairly elongated and offset system to make any biases more obvious. A 2D fit successfully recovered the slope of the outer component ($\beta_{fit}=0.4$). We then attempted to fit the data using a 1D approach. We initially extracted a profile centered on the brightest point in the group (the central component). This gave a profile with a shoulder and a clear central excess. This profile was fitted using QDP with a β -profile plus a constant background. Initially we fitted to the full profile, giving a value of $\beta_{fit} \approx 0.7$. We then progressively excluded the central regions and refitted the data. The fitted value of β_{fit} rose to a peak of ≈ 0.9 before dropping as a larger central region was excluded. Thus it is possible, with the 1D approach used by MZ98, to significantly overestimate the true value of β_{fit} .

To decide whether the models of MZ98 referred to in Table 4 provide an acceptable fit to our data, we carried out a series of two-component fits with the index and core radius frozen at the MZ98 values. The components were also constrained to be circular and centred in the same place. The Cash values for these models were then compared to the best fitting values derived earlier. The differences between the Cash statistic values are shown in the final column of Table 4. As can be seen, the models using the MZ98 parameters generally fall well outside the 99% confidence regions of our best fitting models (which corresponds to $\Delta C=-20.1$). Hence it appears that our more sophisticated models do represent the data significantly better.

The most important difference in the surface brightness results is apparent in the β_{fit} value of the extended component. MZ98 obtain values consistent with $\beta_{fit} \approx 1$ whereas the values obtained here mostly lie in the region 0.4-0.5, with a median value for the extended component of $\beta_{fit} = 0.46$.

MZ98 obtain lower values of β_{fit} when fitting single-component models, but find that the extended components

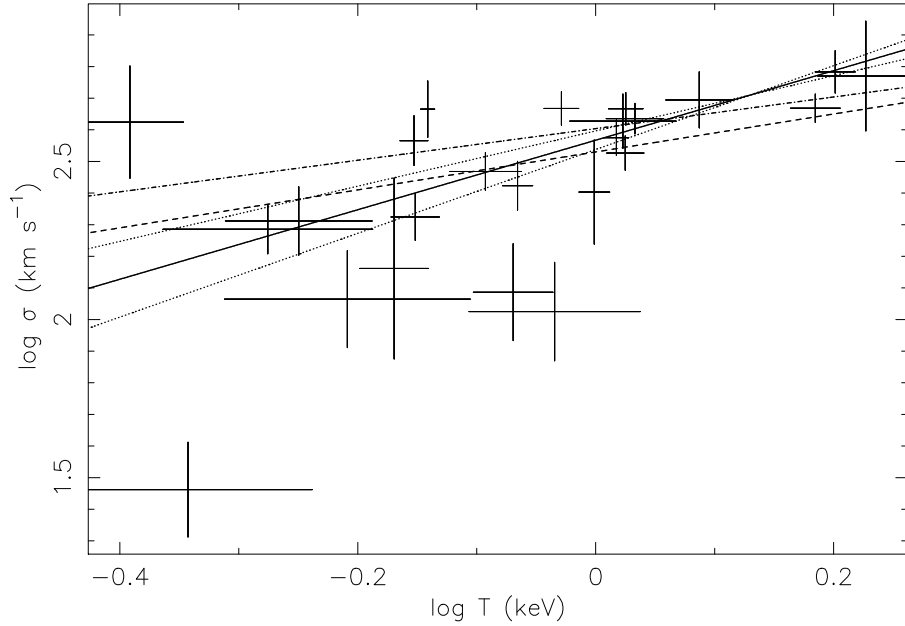


Figure 9. The relationship between group velocity dispersion, σ and temperature. The best fit to the data is shown as the solid line with the one sigma error bounds marked by the dotted lines. The extrapolation of the cluster relation (White et al. 1997) is shown as the dashed line. The dot-dashed line shows the locus along which $\beta_{spec} = 1$.

Table 4. A comparison of the two-component models fitted by Mulchaey & Zabludoff (1998) with those from this work. β_{fit} and core radius values of the extended component for both sets of models are listed. The final column gives the difference in Cash statistic between the two models as fitted to our data; the negative sign indicating that the model fitted here gives the better fit.

Group	M&Z β_{fit}	M&Z core radius (arcmin)	This work β_{fit}	This work core radius (arcmin)	ΔC
NGC 533	0.83	8.15	0.74	10.2	-122.5
NGC 741	1.00	14.08	0.39	0.1	-45.1
NGC 2563	0.86	11.15	0.40	2.6	-26.4
NGC 3091	0.68	3.61	0.41	0.1	-41.0
NGC 4761	0.63	9.00	0.36	0.1	-129.2
NGC 5846	0.83	13.93	0.58	0.84	-263.7

fit with systematically higher β_{fit} when a second component is included (this sort of effect was reproduced in our simulations mentioned earlier). The same effect is noted for a sample of clusters by Mohr et al. (1999), who give a useful discussion of the effect. Since core radius and β_{fit} are strongly positively correlated when fitting (i.e. models with larger cores and higher β_{fit} can give rather similar profiles to those with lower values of both parameters), the presence of a central excess will force r_{core} towards lower values and hence decrease β_{fit} , unless an additional component is included in the model to account for the central excess.

Interestingly, we do not find this to be the case in general, for our analysis. For the subset of our groups with two-component fits, the median value of β_{fit} for the single-component fits is 0.47 (i.e. just steeper than for the two-component fits). Individually, some groups (e.g. NGC533) have a steeper profile when the two-component model is

used, and some (e.g. NGC4761) have a flatter profile. The distinction appears to be that the argument of Mohr et al. (1999) applies to systems for which the *extended* component dominates over most of the range of the fitted data. In this case, the presence of a central component acts to slightly modify the extended component fit, by reducing both r_{core} and β_{fit} . NGC2563 in Fig.3 is such an example. However, for systems where the *central* component is more dominant, such as NGC3091 in Fig.3, the single component fit is a compromise between a steeper central component, and a flatter extended one, so that the result is to *increase* β_{fit} , relative to the extended component.

Fig.10 shows the relationship between the β_{fit} values from one and two-component models for the eight systems from our sample with well-fitting two-component profiles. The solid line splits the graph into two areas. In the upper left area the two-component fit has a steeper profile

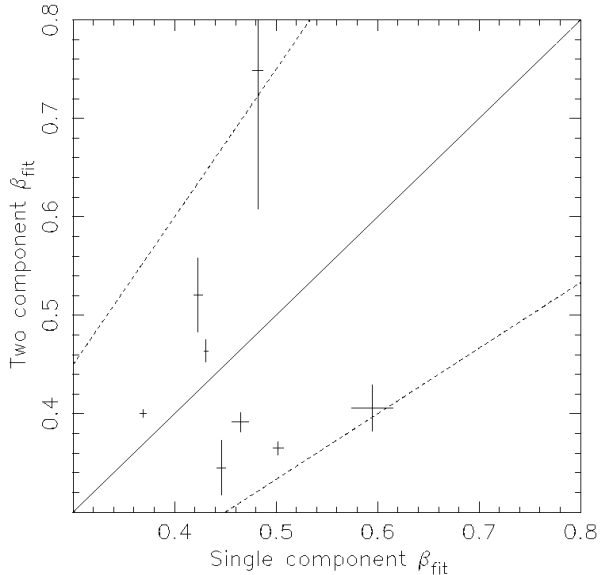


Figure 10. Relationship between the single-component β_{fit} value and the extended component β_{fit} value from the two-component fit. The groups shown are the eight systems with the best fitting two-component models.

than the single-component fit, in the lower right area the reverse is true. As can be seen, the single-component fits lead to overestimates and underestimates of β_{fit} , relative to the two-component results, in equal numbers of cases. The two dashed lines delineate the region in which the two-component fit differs from the single-component fit by less than $\pm 50\%$. As can be seen the two-component models generally have β_{fit} values for the extended component within 50% of the single-component fit. The small nominal errors on the single-component β_{fit} values in the figure are misleading, since they result from calculating errors on a poor fit.

The slope of the $L : T$ relation for our group sample is significantly steeper than the cluster relation. This is in contrast to the results of MZ98, who find that the $L : T$ relation for their sample of nine groups is consistent with the cluster relation. However they had too few points to fit to the group sample alone, so they added a large cluster sample in order to determine the best fit line. If the $L : T$ relation is turning over at a temperature of ≈ 1 keV, as is suggested by Fig.7, then it is to be expected that the line fitted through a combined group and cluster sample would not differ greatly from the cluster relation.

Values of β_{spec} derived by MZ98 for their groups lead them to conclude that $\beta_{spec} \sim 1$, whereas we see evidence for a drop in β_{spec} for low temperature systems (Fig. 9). This difference appears to result from two factors. Firstly, four of the nine common groups are found in the region ($T \gtrsim 1$ keV) where our groups are generally consistent with $\beta_{spec} \sim 1$. So this only leaves five systems in which MZ98 could have noted a drop in β_{spec} . Secondly, our values of β_{spec} appear to be typically about 10% lower than those of MZ98. For the nine groups in common, we derive a mean value of $\langle \beta_{spec} \rangle = 0.78$ compared to $\langle \beta_{spec} \rangle = 0.87$ for MZ98. Since we use the same velocity dispersions, the dif-

ference results from the derived gas temperatures. This difference may arise from the fact that for most groups MZ98 extract their spectral data from within a larger radius, and given the tendency towards a decline in temperature with radius apparent in many systems in Fig.1, this should result in temperatures somewhat lower than ours. This interpretation is supported by the fact that our temperatures are in good agreement with those derived in the study of Mulchaey et al. (1996), in which similar extraction radii were used for systems common to the two studies.

7 DISCUSSION

This survey of X-ray bright, loose galaxy groups represents the largest detailed study of their properties to date. This allows a comparison with the properties of richer clusters, and we have been able to show that three effects are apparent in low temperature systems: steepening of the $L : T$ relation, steepening of the $\sigma : T$ relation (i.e. lower β_{spec} values in groups), and flatter surface brightness profiles in groups. We find that the contrary results of MZ98 appear to be due to the small size of their sample, coupled with their somewhat less sophisticated analysis of the surface brightness distributions.

The general nature of these three departures from cluster trends are in good agreement with the expectations from preheating models, in which energetic winds from forming galaxies raise the entropy of intergalactic gas and inhibit its collapse into the smaller potential wells of galaxy groups (Metzler & Evrard 1994; Cavaliere, Menci & Tozzi 1997; Cavaliere, Menci & Tozzi 1999; Ponman et al. 1999; Metzler & Evrard 1999; Balogh, Babul & Patton 1999). This increase in gas entropy primarily acts to reduce the gas density in the central regions of low mass systems, flattening their surface brightness profiles and reducing their X-ray luminosity. The enhanced entropy also leads to some increase in gas temperature, resulting in a value of β_{spec} less than unity.

The slope of the $L : T$ relation, $L \propto T^{4.9 \pm 0.8}$, is flatter than the index of 8.2 ± 2.7 derived for Hickson groups by Ponman et al. (1996), however the error from the HCG sample was very large, so the difference in slopes is not significant (1.2σ). The present, much more accurate determination of the $L : T$ slope, is in excellent agreement with the asymptotic relation $L \propto T^5$ derived in the low temperature limit by the semi-analytical models of Cavaliere et al. (1997) and Balogh et al. (1999). These two treatments make somewhat different simplifying assumptions about the physics of the heating of the intracluster gas, but both obtain similar slopes in the limit of isentropic gas (i.e. where shock heating becomes negligible).

This result has to be quite robust to detailed model assumptions, since an approximate result $L \propto T^{4.5} \Lambda(T)$, where $\Lambda(T)$ is the cooling function, is easily derived by combining the scaling relations $T \propto M/R$ (from hydrostatic equilibrium), $M \propto R^3$ (for systems virialising at a given epoch), $\rho_{gas} \propto T^{3/2}$ (for constant entropy gas) and $L \propto \rho_{gas}^2 \Lambda(T) R^3$. For bremsstrahlung, $\Lambda(T) \propto T^{1/2}$, so that one obtains $L \propto T^5$. In practice, at $T \sim 1$ keV the cooling function is flatter than $T^{1/2}$, due to the increasing contribution of metal lines at low temperatures, and so the ex-

pected relation flattens somewhat towards $L \propto T^{4.5}$. The good agreement between this isentropic result and our observations lends strong support to the result of Ponman et al. (1999), that the gas entropy tends towards a constant ‘floor’ value, set by preheating, in low temperature systems.

Within the above picture, the significant scatter seen in our $L : T$ relation is expected to be primarily due to different star formation and merging histories of the groups. It has also been shown (Fabian et al. 1994) that scatter in the cluster $L : T$ relation is correlated with the strength of the emission associated with a cooling flow. Lower temperature gas (at a given density) has a shorter cooling time, and it is apparent from Fig.1 that many of these groups do contain cooling flows. Hence some $L : T$ scatter can also be attributed to the presence of cooling flows in the sample.

Another consequence of the effect of galaxy winds is that if winds have injected extra energy into the intragroup medium then a greater proportion of the energy of the system should be found in this hot gas. However, this extra energy could manifest itself in the form of extra thermal energy, or higher gravitational potential energy of the gas. The models of Cavaliere et al. (1999) and Balogh et al. (1999), and the N-body+hydrodynamical simulations of Metzler & Evrard (1999), all indicate that for systems with $T > 1$ keV, the energy is taken up in flattening the gas distribution, with very little effect on gas temperature. Unfortunately, the simulations of Metzler & Evrard (1999) do not extend to lower temperatures, but the models of Cavaliere et al. (1999) and Balogh et al. (1999) both predict that at $T \lesssim 0.8$ keV, systems depart rather suddenly from the cluster $M : T$ relation, with T flattening out at a minimum value. This must necessarily happen, since (in the absence of significant cooling) the gas temperature cannot drop below the level to which it was preheated, since its density will have increased as it settles into the group potential.

The observed $\sigma:T$ relation for our groups (Fig.9), is noisy, but there is a rather clear pattern whereby $\beta_{spec} \approx 1$ for $T \gtrsim 1$ keV, but drops to lower values for cooler systems. For example, the median β_{spec} for our nine groups with $T < 0.8$ keV is 0.44. This behaviour is just what the models predict for preheating temperatures ~ 0.5 keV.

The $L : \sigma$ relation for our group sample is slightly flatter than the cluster relation as determined by White et al. (1997), although the errors on the slope of the loose group sample are large and as a result the difference is not statistically significant. This might suggest that the group $L:\sigma$ relation is an extension of the cluster trend. However, if as argued above, preheating has substantially reduced the luminosity of the groups, then the velocity dispersion must also be lower than expected, otherwise a steepening of the $L : \sigma$ relation, similar to that seen in $L : T$, would be observed.

Bird et al. (1995) have suggested that velocity dispersion should be reduced for lower mass systems due to the effects of dynamical friction, which is more effective in lower mass systems due to their lower velocity dispersion. Loss of orbital energy will lead to a reduction in orbital velocity provided that the potential is less steep than a singular isothermal potential in the inner regions. This would be the case for either a King-like potential, with a flat core, or for potentials of the form introduced by Navarro, Frenk & White (1997), which tend to $\rho \propto r^{-1}$ at small radii. How-

ever it must be remembered that the velocity dispersions of the groups in this sample are drawn from three different sources, and may be based on only a small number of group galaxies, so that statistical errors are large. Zabludoff & Mulchaey (1998) find that when they add the velocities of fainter group galaxies to their redshift samples, the velocity dispersions they derive may increase by a factor of 1.5 or more. This is qualitatively consistent with expectations from dynamical friction, since the orbits of more massive galaxies should decay more quickly, and hence their velocity dispersion would drop below that of fainter group members.

The results on the asymptotic slope of the X-ray surface brightness in groups derived here, confirms and quantifies the result of Ponman et al. (1999), who showed that surface brightness is progressively flattened in low temperature systems. This trend is in accord with preheating models, as discussed above, although our median value of $\beta_{fit} = 0.46$ is a little lower than the values $\beta_{fit} \approx 0.5-0.6$ predicted by the models of Metzler & Evrard (1999) and Cavaliere et al. (1999) for $T \sim 1$ keV.

The situation in clusters is still a matter of debate. Arnaud & Evrard (1999) collect together results from the literature, and find a clear trend in β_{fit} with temperature, as can be seen in Fig.4. However, Mohr et al. (1999) find that two-component fits are required to adequately represent most cluster profiles, and that the results from such fits show no trend in the value of β_{fit} for the extended cluster component. They conclude that results such as those of Arnaud & Evrard (1999) arise from biases due to the inappropriate use of single β -model profiles. On the other hand, we *have* accounted for the central component, but still find that β_{fit} is substantially lower in groups than the value of 2/3 found for clusters by Mohr et al. (1999).

The resolution of this situation probably lies in the temperature ranges covered. The analysis of Ponman et al. (1999) is model-independent, in that it involved simply over-laying the scaled surface brightness profiles. This shows that flattening of the profiles sets in at temperatures $T \lesssim 3$ keV. Since the sample of Mohr et al. (1999) includes only a single cluster with $T < 3$ keV, the lack of trend in β_{fit} observed within their sample, and the much flatter profiles observed in our sample, are both consistent with the Ponman et al. (1999) results.

Finally, we wish to emphasize that an important implication of the flat X-ray profiles of groups, coupled with their generally low surface brightness compared to clusters, is that one must be very careful in drawing conclusions about properties such as gas mass, gas fraction etc. on the basis of analyses confined to ‘detection radii’. For example Mulchaey et al. (1996) conclude that masses of gas in groups are typically lower than the mass in galaxies, on the basis of analyses within the region of detectable X-ray emission, which in many cases is only ~ 200 kpc. Such results have important implications. For example, Renzini (1997) has used them to argue that the iron mass to light ratio in groups is much lower than that in clusters, and that it is therefore difficult to explain how clusters can be assembled through group mergers.

It can be seen from Fig.6 that under the assumption that our β -model fits can be extrapolated to R_V , less than 50% of the X-ray luminosity of the system is contained within 200 kpc for typical groups. Now the asymp-

otic power law behaviour of surface brightness at large r is $S(r) \propto r^{1-6\beta}$, whilst the corresponding density profile (in the approximation of isothermal gas) is $\rho_{gas} \propto r^{-3\beta}$. Hence the density profile is even flatter, and the fraction of the total gas mass contained within $r = 200$ kpc will be considerably *less* than 50%. The flat gas profiles mean that the gas fractions of groups rise strongly with radius, so that very different results might be obtained if our instruments were sufficiently sensitive to detect group emission out to R_V , a possibility which should be realised with the launch of XMM.

8 CONCLUSIONS

We have carried out detailed analysis of *ROSAT* PSPC data for 24 X-ray bright galaxy groups. Temperatures and bolometric luminosities have been derived for each group, and surface brightness profiles modelled in some detail. In agreement with previous studies we find evidence for the presence of two components in the surface brightness profiles of many of the groups. When present, the central component is coincident with the position of a central galaxy, suggesting that it may be due to the halo of the galaxy, or to a cooling flow focused onto the central galaxy.

The surface brightness profiles of groups are significantly flatter than those of galaxy clusters. For a subsample of the groups with the best data, the steepness of the surface brightness profiles, as measured by the parameter β_{fit} , appear to show a trend with mass when combined with cluster data. This result is consistent with the idea that galaxy winds have significantly affected the state of the intergalactic medium in low mass systems.

The relation between the X-ray luminosity and temperature for galaxy groups is also derived. This relation is found to be significantly steeper than that derived for galaxy clusters. The action of galaxy winds flattening surface brightness profiles would reduce the luminosity of the gas, due to the luminosity dependence on the square of the density, thus causing a steepening of the $L : T$ relation for lower mass systems. Further evidence for this scenario is provided in the relation between velocity dispersion and temperature. The $\sigma : T$ relation shows that for lower mass systems the specific energy in the gas is greater than the specific energy in the galaxies, suggesting that there has been energy injection in these systems. An encouraging level of agreement is apparent between our results and recent models and simulations of the effects of preheating by galaxy winds.

9 ACKNOWLEDGEMENTS

We thank Alex Deakin for his work in the early stages of this project, John Mulchaey for interesting discussions about the X-ray properties of groups, and the referee for suggesting several improvements to the paper. Edward Lloyd-Davies and Bruce Fairley provided help and advice on the data analysis and read several versions of this manuscript.

SFH acknowledges financial support from the University of Birmingham. This work made use of the Starlink facilities at Birmingham, the LEDAS database at Leices-

ter, the NASA/IPAC Extragalactic Database (NED), and images from the STScI Digitized Sky Survey.

REFERENCES

- Allen S. W., Fabian A. C., 1998, *MNRAS*, 297, 57
- Arnaud M., Evrard A. E., 1999, preprint, astro-ph/9806353
- Arnaud M., 1994, in Seitter W., ed, *Cosmological Aspects of X-ray Clusters of Galaxies*. Kulwer, Dordrecht, p. 197
- Balogh M. L., Babul A., Patton D. R., 1999, preprint, astro-ph/9809159
- Bird C. M., Mushotzky R. F., Metzler C. A., 1995, *ApJ*, 453, 40
- Buote D. A., Fabian A. C., 1998, *MNRAS*, 296, 977
- Burns J., Hanisch R. J., White R. A., Nelson E. R., Morrisette K. A., Moody J. W., 1987, *AJ*, 94, 587
- Burns J. O., Ledlow M. J., Loken C., Klypin A., Voges W., Bryan G. L., Norman M. L., White R. A., 1996, *ApJ*, 467, L49
- Burstein D., 1990, *Rep. Prog. Phys.*, 53, 423
- Cash W., 1979, *ApJ*, 228, 939
- Cavaliere A., Menci N., Tozzi P., 1997, *ApJ*, 484, L21
- Cavaliere A., Menci N., Tozzi P., 1999, preprint, astro-ph/9810498
- Dell'Antonio I. P., Geller M. J., Fabricant D. G., 1994, *AJ*, 107, 427
- Doe S. M., Ledlow M., Burns J. O., White R. A., 1995, *AJ*, 110, 46
- Fabian A. C., Crawford C. S., Edge A. C., Mushotzky R. F., 1994, *MNRAS*, 267, 779
- Finoguenov A., Ponman T. J., 1999, *MNRAS*, in press, astro-ph/9901100
- Fixsen D. J., Cheng E. S., Gales J. M., Mather J. C., Shafer R. A., Wright E. L., 1996, *ApJ*, 473, 576
- Fukazawa Y., Makishima K., Tamura T., Ezawa H., Xu H., Ikebe Y., Kikuchi K., Ohashi T., 1998, *PASJ*, 50, 187
- Fukugita M., Hogan C. J., Peebles P. J. E., 1998, *ApJ*, 503, 518
- Hickson P., 1982, *ApJ*, 255, 382
- Hwang U., Mushotzky R. F., Burns J. O., Fukazawa Y., White R. A., 1999, *ApJ*, 516, 604
- Ikebe Y. et al., 1997, *ApJ*, 481, 660

- Ledlow M. J., Loken C., Burns J. O., Hill J. M., White R. A.,
1996, *AJ*, 112, 388
- Mahdavi A., Boehringer H., Geller M. J., Ramella M., 1997,
ApJ, 483, 68
- Markevitch M., 1998, *ApJ*, 504, 27
- Metzler C. A., Evrard A., 1994, *ApJ*, 437, 564
- Metzler C. A., Evrard A., 1999, preprint, astro-ph/9710324
- Mewe R., Lemen J. R., van den Oord G. H. J., 1986, *A&AS*,
65, 511
- Mohr J. J., Mathiesen B., Evrard A. E., 1999, *ApJ*, in press,
astro-ph/9901281
- Mulchaey J. S., Zabludoff A. I., 1998, *ApJ*, 496, 73
- Mulchaey J. S., Davis D. S., Mushokzky R. F., Burstein D.,
1993, *ApJ*, 404, L9
- Mulchaey J. S., Davis D. S., Mushotzky R. F., Burstein D.,
1996, *ApJ*, 456, 80
- Navarro J. F., Frenk C. S., White S. D. M., 1995, *MNRAS*,
275, 720
- Navarro J. F., Frenk C. S., White S. D. M., 1997, *ApJ*, 490,
493
- Nolthenius R., 1993, *ApJS*, 85, 1
- Ponman T. J., Bertram D., 1993, *Nature*, 363, 51
- Ponman T. J., Bourner P. D. J., Ebeling H., Bohringer H.,
1996, *MNRAS*, 283, 690
- Ponman T. J., Cannon D. B., Navarro J. F., 1999, *Nature*,
397, 135
- Price R., Burns J. O., Duric N., Newberry M. V., 1991, *AJ*,
102, 14
- Ramella M., Geller M. J., Huchra J. P., 1990, *ApJ*, 353, 51
- Renzini A., 1997, *ApJ*, 488, 35
- Snowden S. L., Mccammon D., Burrows D. N., Mende-
hall J. A., 1994, *ApJ*, 424, 714
- Stark A. A., Gammie C. F., Wilson R. W., Bally J.,
Linke R. A., Heiles C., Hurwitz M., 1992, *ApJS*, 79,
77
- Tully R. B., 1987, *ApJ*, 321, 280
- White D. A., Jones C., Forman W., 1997, *MNRAS*, 292, 419
- Xu H., Ezawa H., Fukazawa Y., Kikuchi K., Makishima K.,
Ohashi T., Tamura T., 1997, *PASJ*, 49, 9
- Zabludoff A. I., Mulchaey J. S., 1998, *ApJ*, 496, 39